Bulletin of the Seismological Society of America, Vol. 83, No. 3, pp. 756–779, June 1993

MODELING TELESEISMIC *P*-WAVE PROPAGATION IN THE UPPER MANTLE USING A PARABOLIC APPROXIMATION

BY M. G. BOSTOCK, J. C. VANDECAR, AND R. K. SNIEDER

ABSTRACT

Teleseismic waves propagating in the upper mantle are subject to considerable distortion due to the effects of laterally heterogeneous structure. The magnitude and scale of velocity contrasts representative of features such as subducted slabs may be such that wave diffraction becomes an important process. In this case forward modeling methods based on high-frequency asymptotic approximations to the wave equation will not accurately describe the wavefield. A method is introduced to model the propagation of teleseismic *P* waves in a laterally heterogeneous upper mantle that accounts for distortion of the initial portion of the wavefield including the effects of multipathing and frequency-dependent diffraction. The method is based on a parabolic approximation to the wave equation that is solved in the time domain on a finite-difference grid which mimics the expected pattern of energy flow in a reference velocity field. Numerical examples for a simple two-dimensional subducting slab model demonstrate the application of the method and illustrate the effects of multipathing and diffraction which dominate waveform distortion at high and low frequencies, respectively.

INTRODUCTION

The principal objective of this study is to introduce a method for modeling waveforms in structurally complex areas of the Earth's upper mantle. On a global scale we find that the most pronounced lateral contrasts in the Earth occur in this region, and in particular at subduction zones where variations in temperature of up to 1000 K are possible over scales of less than 100 km. The associated contrasts in seismic velocity must occur over similar distances and are estimated to represent a 3% to 10% deviation from radially stratified Earth models (Silver *et al.*, 1988; Lay, 1991). Velocity variations of this magnitude may have significant effects on the propagation of seismic waves, on travel times (e.g., VanDecar and Crosson, 1990; Spakman, 1991), amplitudes (Thomson and Gubbins, 1982; VanDecar *et al.*, 1990), and more generally on the character of observed waveforms (Davies and Julian, 1972; Sleep, 1973; Silver and Chan, 1986; Gubbins and Snieder, 1991). For teleseismic waves this magnitude of velocity contrast and the scales over which variations can occur imply that techniques based on asymptotic ray theory may not adequately describe relevant aspects of the observed wave field. More specifically, frequency-dependent effects or diffractions become important and the degree to which any asymptotic method (e.g., Gaussian beams, Maslov theory) can account for this class of wave interaction is not clear (see Cormier, 1989). As a consequence, accurate modeling of waveforms through subduction zone environments has been limited to a large extent to finite difference calculations for some two-dimensional (2D) models (Vidale, 1987; Vidale and Garcia-Gonzalez, 1988).

Full waveforms have the potential to provide a wealth of information concerning the structure of the subducted lithosphere in the upper mantle and should be exploited to shed light on the dynamic processes which are operative at these

depths. Difficulties in the analysis of full waveforms arise, however, due to the complexity of the multipathing and diffraction processes which occur in an environment as complex as a subduction zone. More specifically we must contend with scattered energy that may potentially arrive from any one of a multitude of possible directions and may have changed identity several times along the way through the processes of mode conversion. Indeed, the problem of full 3D modeling of elastic waveforms over reasonable propagation distances is, at the present time, computationally intractable. It seems reasonable therefore to set our sights on a more immediately attainable goal: an accurate description of the first few cycles of *P*-wave energy. From physical considerations, we know that the energy in this initial portion of the seismogram will, in most cases, have traversed a reasonably well defined region between source and receiver, or specifically a region with frequency-dependent volume but centered in some loose sense about the geometrical ray. In addition, with the exception of interactions in the very near vicinity of the source and the receiver, we can avoid the analysis of scattered *S*-wave contributions to the *P*-wave field since they will arrive considerably later in the seismogram.

In the following sections we outline a method to simulate teleseismic *P* waves in the upper mantle based on a parabolic approximation to the wave equation which allows us to model diffraction effects that are not adequately described by ray-theoretical techniques, and which is much less computationally intensive than a full finite-difference treatment of the elastic case. We then proceed to apply the method in a simple 2D model of a subduction zone to demonstrate its application and illustrate the effects of diffraction on *P*-waveforms at different frequencies. The application and extension of the method to the problem of modeling teleseismic *P* waves in a realistic, 3D model of a subduction zone is the subject of a paper in preparation.

A Scalar Wave Equation for the Initial *P* Wave Arrivals

We begin with the equation of elastic wave motion in generally anisotropic, heterogeneous media in the absence of sources

$$\rho \frac{\partial^2 u_i}{\partial t^2} = (c_{ijkl} u_{k,l})_{,j}, \tag{1}$$

where u_i is the displacement, c_{ijkl} is the elastic modulus tensor and ρ is density. We will confine our attention to the study of isotropic, heterogeneous media and so, by employing the constitutive relation

$$c_{ijkl} = \lambda \delta_{ij} \delta_{kl} + \mu(\delta_{ik} \delta_{jl} + \delta_{il} \delta_{jk}), \tag{2}$$

we write (1) as

$$\rho \frac{\partial^2 u_i}{\partial t^2} = (\lambda + 2\mu) u_{j,ij} + \mu u_{i,jj} + \lambda_{,i} u_{j,j} + \mu_{,j}(u_{i,j} + u_{j,k}) \tag{3}$$

where λ and μ are the Lamé parameters. This expression can be written in a more convenient form by adopting vector notation and exploiting various vector

identities to yield

$$\frac{\partial^2}{\partial t^2}\mathbf{u} = \alpha^2\nabla(\nabla\cdot\mathbf{u}) - \beta^2\nabla\times\nabla\times\mathbf{u} + \frac{\nabla\lambda}{\rho}\nabla\cdot\mathbf{u} + \frac{\nabla\mu}{\rho}\times(\nabla\times\mathbf{u}) + 2\left(\frac{\nabla\mu}{\rho}\cdot\nabla\right)\mathbf{u}. \tag{4}$$

We note that in homogeneous media the last three terms vanish and we can associate the remaining equation with the motion of P and S waves propagating independently with velocities α and β, respectively, where

$$\alpha = \left(\frac{\lambda + 2\mu}{\rho}\right)^{1/2} \tag{5}$$

and

$$\beta = \left(\frac{\mu}{\rho}\right)^{1/2}. \tag{6}$$

The independence of P and S waves in homogeneous media can be demonstrated by alternately taking the divergence and curl of equation (4) (while ignoring the last three terms) and employing the definition of the dilatation θ and the rotation vector $\mathbf{S}$ where

$$\theta = \nabla\cdot\mathbf{u}, \tag{7}$$

$$\mathbf{S} = \nabla\times\mathbf{u}. \tag{8}$$

In heterogeneous media, however, we must apply the divergence and curl to all terms in (4) and in so doing we retrieve two equations which are coupled in θ and $\mathbf{S}$. By considering only first-order terms in the gradients of material properties, that is ignoring second derivatives and products of first derivatives, an approximation to this system can be conveniently written as

$$\frac{1}{\alpha^2}\frac{\partial^2\theta}{\partial t^2} = \nabla^2\theta + (2\mathbf{g}_\alpha + \mathbf{g}_\rho)\cdot\nabla\theta - \left(\frac{\beta}{\alpha}\right)^2(2\mathbf{g}_\beta + \mathbf{g}_\rho)\cdot\nabla\times\mathbf{S} \tag{9}$$

and

$$\frac{1}{\beta^2}\frac{\partial^2\mathbf{S}}{\partial t^2} = \nabla^2\mathbf{S} - \mathbf{g}_\beta\times(\nabla\times\mathbf{S}) + \left[(\mathbf{g}_\beta + \mathbf{g}_\rho)\cdot\nabla\right]\mathbf{S} + \left[2\mathbf{g}_\beta + \left(2 - \left(\frac{\alpha}{\beta}\right)^2\right)\mathbf{g}_\rho\right]\times\nabla\theta. \tag{10}$$

Here we have adopted the notation of Landers and Claerbout (1972) (note also a similar formulation by Ben-Menahem and Beydoun (1985)) and employed the

following abbreviated variables:

$$\mathbf{g}_\alpha = (\nabla\alpha^2)/\alpha^2 \tag{11a}$$

$$\mathbf{g}_\beta = (\nabla\beta^2)/\beta^2 \tag{11b}$$

$$\mathbf{g}_\rho = \nabla\rho/\rho. \tag{11c}$$

Let us now examine equation (9) in more detail. It represents a scalar wave equation for the dilatation θ but it differs from the corresponding equation for a homogeneous medium by the presence of the last two terms. The first of these terms involves gradients in the square of the *P*-wave velocity and density, and accounts to first order for *P* to *P* scattering processes. The second term contains the rotation vector **S** and describes first-order scattering contributions to the *P*-wave field arising from mode conversion of *S* waves due to gradients in rigidity and density. Note here that by first order we mean the effects of first-order gradients in material properties, not the single scattering contribution from a region of heterogeneity. These equations remain valid while the gradients in material properties are "smooth" as defined by Ben-Menahem and Beydoun (1985). These authors employed this terminology to distinguish such gradients from the "weak" variations in material properties which are required in order that ray theory be valid and that *P* and *S* waves can be viewed as propagating independently. Now consider the physical nature of the these contributions in the time domain. We can write the first-order *S*-wave contribution to the *P*-wave field θ_S using representation theorems (see e.g., Aki and Richards, 1980) as

$$\theta_S(\mathbf{x}, t) = \int dt' \int d\mathbf{x}' \left[\frac{\beta(\mathbf{x}')}{\alpha(\mathbf{x}')}\right]^2 \left[2\mathbf{g}_\beta(\mathbf{x}') + \mathbf{g}_\rho(\mathbf{x}')\right] \cdot \nabla \times \mathbf{S}(\theta, \mathbf{x}', t') G(\mathbf{x}, t|\mathbf{x}', t'), \tag{12}$$

where $G(\mathbf{x}, t|\mathbf{x}', t')$ is the Green's function for the scalar wave equation

$$\frac{1}{\alpha(\mathbf{x})^2} \frac{\partial^2 G(\mathbf{x}, t|\mathbf{x}', t')}{\partial t^2} = \nabla^2 G(\mathbf{x}, t|\mathbf{x}', t') + \delta(\mathbf{x} - \mathbf{x}')\delta(t - t'). \tag{13}$$

In this form it is apparent that contributions to the *P*-wave field resulting from scattering of the direct *S* wave arrive at times greater than $\int_{\mathbf{x}_0}^{\mathbf{x}'} ds\beta^{-1} + \int_{\mathbf{x}'}^{\mathbf{x}} ds\alpha^{-1}$, where $\mathbf{x}'$ and $\mathbf{x}$ are the coordinates of the scattering region and the observer relative to an origin $\mathbf{x}_0$ coinciding with the earthquake source, and s is the distance along the raypath connecting the appropriate points as shown in Figure 1. If we ignore *S*-*P* scattering in the near source regime, $|\mathbf{x}' - \mathbf{x}_0| \ll |\mathbf{x} - \mathbf{x}'|$, then the first cycles of *P*-wave energy at $\mathbf{x}$ are not affected by this scattering. In a similar fashion we will choose to ignore scattering processes in the near receiver vicinity, $|\mathbf{x}' - \mathbf{x}_0| \gg |\mathbf{x} - \mathbf{x}'|$, which would allow for *S*-wave contamination to the initial energy via scattering of the direct *P* wave. The dependence of the *S*-wave field on θ is shown explicitly in (12) to indicate the coupling of equations (9) and (10), and that there is, of course, a continual exchange of energy between *P* and *S* waves propagating in a generally hetero-

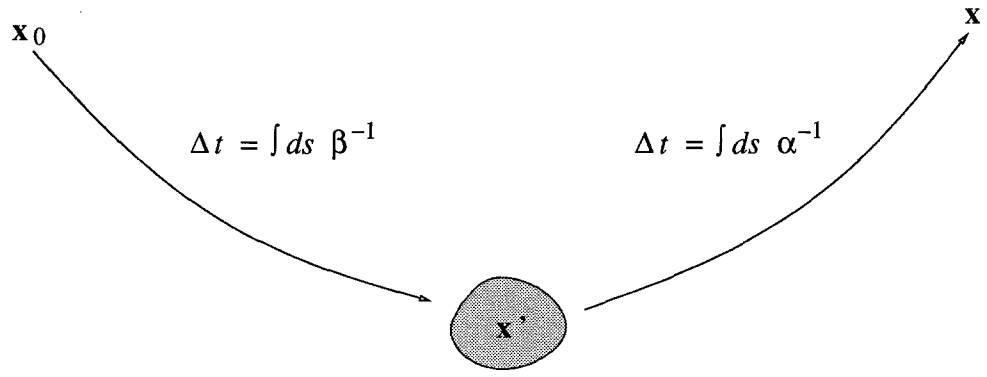

FIG. 1. With the exception of conversions originating near the source $\mathbf{x}_0$, energy scattered into P from the direct S wave at some point $\mathbf{x}'$ should arrive at considerably later times than the direct P wave at a point of observation $\mathbf{x}$.

geneous medium. This means that there are S-wave contributions to the P-wave train in the initial energy but they are of second order and involve conversion from P to S and back to P. Implicit in this feedback process is the energy which is lost from P due to conversion to S. If we constrain our material property perturbations (11) to be of order ϵ then it is not difficult to show that S-wave contributions arising through P to S to P conversion must be of order ϵ^2 and hence can be ignored over the first few cycles of P-wave energy. In this sense our formulation is essentially a single scattering approximation as we are ignoring the energy loss in the initial P wave which accrues from conversion to S.

Thus we will restrict our attention to the first few cycles of P-wave energy and neglect the last term in (9) which results in a simple scalar equation describing the initial P-wave motion in media with smooth gradients in material properties, or specifically

$$\frac{1}{\alpha^2}\frac{\partial^2\theta}{\partial t^2} = \nabla^2\theta + (2\mathbf{g}_\alpha + \mathbf{g}_\rho)\cdot\nabla\theta. \tag{14}$$

One further point to note is the way in which scattering from smooth gradients in material properties enters into the final term of (14). In addition to the ray geometrical amplitude growth/decay that a waveform experiences due to velocity and density gradients in the direction of propagation, this term describes frequency-dependent scattering phenomena which result from interactions in directions transverse to propagation. In the event that material variations are smooth, forward scattering or "transmission" will dominate over back scattering or "reflection" (see e.g., Aki and Richards, 1980). This has important implications for the manner in which we choose to solve (14).

Despite its simplicity relative to the coupled system in (9) and (10), a full finite-difference treatment of equation (14) in a laterally heterogeneous upper mantle environment is not computationally attractive, nor is it necessarily warranted as we are interested only in the first few cycles of arriving energy and we are assuming that gradients in material properties, while important, are smooth so that only forward scattering is significant. In the following sections we will further simplify equation (14) by adopting a time domain parabolic

approximation which allows us to formulate the problem in terms of a one-way wave equation which is efficient and relatively simple to solve numerically.

Parabolic Approximations to Wave Equations

In deriving a parabolic approximation or "one-way" wave equation we are forced to make some *a priori* assumptions regarding the nature of the wave field we wish to model. In particular it is necessary to adopt a coordinate system in which one of the coordinate axes roughly coincides with the dominant direction of propagation. In this section we illustrate the essential ideas involved in the derivation of a time domain parabolic approximation by examining the behavior of solutions to the wave equation in (14) for a simple 2D Cartesian geometry, where the wave equation becomes

$$\frac{1+\delta(x,y)}{\alpha_0^{\,2}}\frac{\partial^2\theta}{\partial t^2}=\frac{\partial^2\theta}{\partial x^2}+\frac{\partial^2\theta}{\partial y^2}+(2\mathbf{g}_\alpha+\mathbf{g}_\rho)\cdot\nabla\theta. \tag{15}$$

Here we consider a medium that is characterized by smooth perturbations $\delta(x, y)$ on a homogeneous reference model with constant slowness α_0^{-1}. In addition we consider a solution which behaves roughly as a plane wave and propagates primarily along a single preferred direction, e.g., x. In frequency domain derivations of parabolic approximations (e.g., Claerbout, 1970), the solution to this equation is usually written as $\theta(x, y, \omega) = \Theta(x, y, \omega) \exp(i\omega x/\alpha_0)$ where $\Theta(x, y, \omega)$ is a slowly varying, modulating function which has been separated from a more rapidly varying phase term. This representation is useful when the medium is smooth and backscattering is negligible. In a homogeneous medium ($\delta = 0$), $\Theta(x, y, \omega)$ would of course remain constant in space and time and represent simply the amplitude of an undistorted plane wave. To derive a time domain expression for the solution we integrate over all frequencies so that

$$\theta(x,y,t)=\int_{-\infty}^{\infty}d\omega\Theta(x,y,\omega)\exp[-i\omega(t-x/\alpha_0)]=\Theta(x,y,t-x/\alpha_0). \tag{16}$$

It is obvious here that if we define the retarded temporal coordinate τ such that

$$\tau = t - x/\alpha_0$$

then $\theta(x, y, t)$ is the inverse Fourier transform of the slowly varying modulation $\Theta(x, y, \omega)$ in τ, or $\Theta(x, y, \tau)$. There are several reasons, however, why it is advantageous to treat the problem directly in the time domain rather than perform the calculation over a full frequency band followed by Fourier transformation. Most importantly, as noted by Claerbout and Johnson (1971), it may be difficult to obtain a sufficiently accurate solution to (16) when subtle features characterize the waveforms under consideration, even with high accuracy over a large frequency band. Low amplitude signal may be obscured by periodicity and parasitic interference patterns caused by higher amplitude energy at other times. Time domain solutions also offer certain advantages from a computational point of view; for example, efficient algorithms may be devised for array processors since there is no need to perform complex arithmetic.

We therefore proceed to solve (15) in the time domain, applying the transfor-

mation to retarded time coordinate τ directly. Using the chain rule this leads to an equation for Θ as

$$\left[\frac{\partial^2\Theta}{\partial x^2} - \frac{2}{\alpha_0}\frac{\partial^2\Theta}{\partial\tau\,\partial x} - \frac{\delta(x,y)}{\alpha_0^2}\frac{\partial^2\Theta}{\partial\tau^2} + (2\mathbf{g}_\alpha + \mathbf{g}_\rho)_x\left(\frac{\partial\Theta}{\partial x} - \frac{1}{\alpha_0}\frac{\partial\Theta}{\partial\tau}\right) + \frac{\partial^2\Theta}{\partial y^2} + (2\mathbf{g}_\alpha + \mathbf{g}_\rho)_y\frac{\partial\Theta}{\partial y}\right] = 0. \quad (17)$$

Note that to this point equation (17) remains equivalent to (15), we have simply chosen to represent the solution in a retarded temporal reference frame which reflects the dominant anticipated phase variation. We now perform a scale analysis to assess the significance of the first five terms. Equation (14) was derived under the assumption that variations in material properties are smooth and vary on a scale length L such that $L \gg \Lambda$ where Λ is the dominant wavelength of the P wave. We note once more that this is consistent with the notion that forward scattering dominates over backscattering. Under these conditions Θ is also slowly varying, and in particular, we expect that it will vary on the same scale length L as the material properties. We observe then that

$$\frac{\partial^2\Theta}{\partial x^2} \propto \frac{1}{L^2}, \qquad \frac{2}{\alpha_0}\frac{\partial^2\Theta}{\partial\tau\,\partial x} \propto \frac{1}{\Lambda L}, \qquad \frac{\delta(x,y)}{\alpha_0^2}\frac{\partial^2\Theta}{\partial\tau^2} \propto \frac{1}{\Lambda^2},$$

$$(2\mathbf{g}_\alpha + \mathbf{g}_\rho)_x\frac{\partial\Theta}{\partial x} \propto \frac{1}{L^2}, \qquad (2\mathbf{g}_\alpha + \mathbf{g}_\rho)_x\frac{1}{\alpha_0}\frac{\partial\Theta}{\partial\tau} \propto \frac{1}{\Lambda L}.$$

We derive a one way wave equation by dropping terms proportional to $1/L^2$ so that we have

$$\left[-\frac{2}{\alpha_0}\frac{\partial^2\Theta}{\partial\tau\,\partial x} - \frac{\delta(x,y)}{\alpha_0^2}\frac{\partial^2\Theta}{\partial\tau^2} - (2\mathbf{g}_\alpha + \mathbf{g}_\rho)_x\frac{1}{\alpha_0}\frac{\partial\Theta}{\partial\tau} + \frac{\partial^2\Theta}{\partial y^2} + (2\mathbf{g}_\alpha + \mathbf{g}_\rho)_y\frac{\partial\Theta}{\partial y}\right] = 0. \quad (18)$$

We are now left with only a first-order derivative in the direction of propagation which allows us to formulate a forward-propagator, finite-difference scheme that is easier to solve numerically than a finite-difference treatment of the full hyperbolic wave equation in (15). We note that equation (18) may be posed in an alternate form by integration with respect to reduced time from negative infinity to a current τ. This removes the temporal derivative in the first term of (18) and is more convenient from the point of view of numerical implementation as will be discussed in a later section.

This form of parabolic equation is known as the 15° approximation (see Claerbout, 1976, 1985) since the effective dispersion relation is a reasonable approximation to that for the full hyperbolic equation over an angular range of 15° from the principal direction of propagation. An attractive feature of the parabolic equation is that the physical significance of each of the remaining terms in (18) is now readily apparent. The $\partial^2\Theta/\partial\tau^2$ term is an advective term

and accounts for delays or advances in the wavefront, the $\partial\Theta/\partial\tau$ term describes the change in amplitude of the wave as it depends on the local material properties, and the $\partial\Theta/\partial y$ and $\partial^2\Theta/\partial y^2$ terms are diffraction terms which account for healing of the wavefront.

Note that the Gaussian beam method (Cerveny and Psencik, 1983), which relies on a similar parabolic approximation to the wave equation, is an asymptotic approximation in frequency and as such is local with all physical quantities calculated along a specific ray. In contrast we will undertake to solve an equation developed in the following sections and similar to (18), on a finite-difference grid, at necessarily greater expense, but which permits a more global treatment of propagation. That is, widely separated elements are allowed to interact with each other through the implementation of the diffraction operator. The accuracy and general performance of the parabolic approximation, in particular the form which we have chosen to implement in this study, is examined in a second paper where synthetic seismograms for several simple models are compared with those computed using full finite differences and Maslov theory.

In his "phase front" approach Haines (1983, 1984a, b) extended the plane wave parabolic treatment to more general classes of heterogeneous media by adopting a curvilinear coordinate system which mimics the general flow of energy through a given medium. It is this class of approach which we will adopt in the following analysis.

A Parabolic Approximation for *P* Waves in the Upper Mantle

The upper mantle of the Earth is characterized by a variation in material properties, and seismic velocities in particular, that is primarily a function of depth. In order that we may implement a parabolic wave equation for P waves propagating in the upper mantle it is necessary that we identify a coordinate system which reflects this dominant variation. Since we are concerned with the transmission effects on the first arrivals we will disregard the effects of velocity discontinuities and concentrate on P-wave velocity models that incorporate the more smoothly varying character of typical upper mantle velocity profiles. A useful reference in this case is the Herrin model shown in Figure 2 along with models PREM and IASPEI for the top 1000 km of the Earth. The implementation of a parabolic approximation to the wave equation in (14) is not critically dependent upon the exact form of the coordinate system adopted as long as one coordinate corresponds reasonably closely with the principal direction of propagation of the anticipated wave field. Bearing this in mind, we note that over most of the top 800 km or so the velocity profiles in Figure 2 can be reasonably well represented in terms of a function that is linear in depth. This suggests that we consider the use of a ray coordinate system for a medium with constant gradient in velocity $\alpha_{LRM}(z)$ as a function of depth

$$\alpha(z) = \alpha_0 + mz. \tag{19}$$

As is well known, ray paths and wave fronts for a point source in this class of media are described by circular arcs and spherical surfaces, and hence may be defined analytically. In addition, a ray coordinate system defined for this class of media is regular everywhere except at the actual location of the defining point source. Although it is not strictly necessary, let us proceed with the development on the basis that our reference coordinate system is constructed for

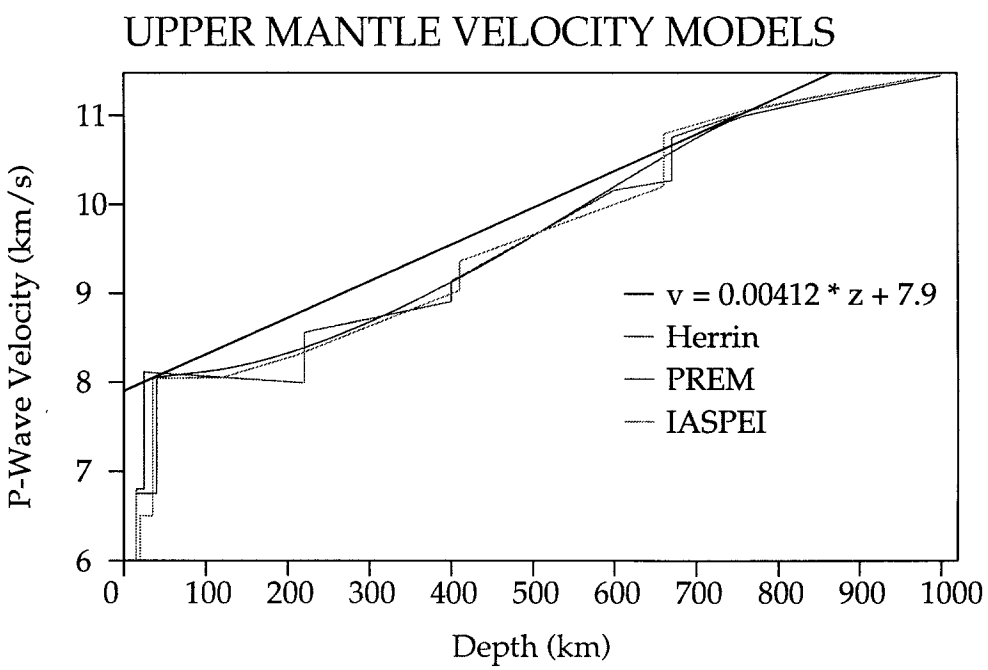

FIG. 2. Various upper mantle *P*-velocity models (*stippled lines*) and a constant gradient *P*-velocity model (*solid line*) over the top 1000 km of the Earth's crust and mantle.

a medium which exhibits a constant velocity gradient with depth as shown in Figure 2. For brevity we shall refer to this "linear reference medium" as LRM.

The most natural choice of reference frame associated with the LRM we have just described is one based on ray coordinates and which incorporates the variables T, ζ, and Φ; where T is the travel time, ζ is the initial angle of a ray measured relative to the z-axis, and Φ is the angle made by the ray in the horizontal plane with respect to some predesignated axis. Note that these three variables constitute an orthogonal curvilinear coordinate system. In the following sections and the numerical examples we will discard the Φ dependence and treat the 2D problem to illustrate implementation of the method. The generalization of the method to 3D is straightforward and comprehensive 3D modeling will be the subject of future study.

Now let us consider the form taken by the wave equation in (14) when referred to this 2D orthogonal curvilinear coordinate system. First note that the terms involving gradient and Laplacian operators in this system are given by

$$\nabla\Theta = \left(\mathbf{n}_T \frac{1}{h_T}\frac{\partial\Theta}{\partial T} + \mathbf{n}_\zeta \frac{1}{h_\zeta}\frac{\partial\Theta}{\partial\zeta}\right), \tag{20}$$

and

$$\nabla^2\Theta = \frac{1}{h_T h_\zeta}\left[\frac{\partial}{\partial T}\left(\frac{h_\zeta}{h_T}\frac{\partial\Theta}{\partial T}\right) + \frac{\partial}{\partial\zeta}\left(\frac{h_\zeta}{h_T}\frac{\partial\Theta}{\partial\zeta}\right)\right]. \tag{21}$$

Here $\mathbf{n}_T$ and $\mathbf{n}_\zeta$ are unit vectors pointing in the directions of increasing T and ζ, and h_T and h_ζ are scale factors associated with the respective coordinates.

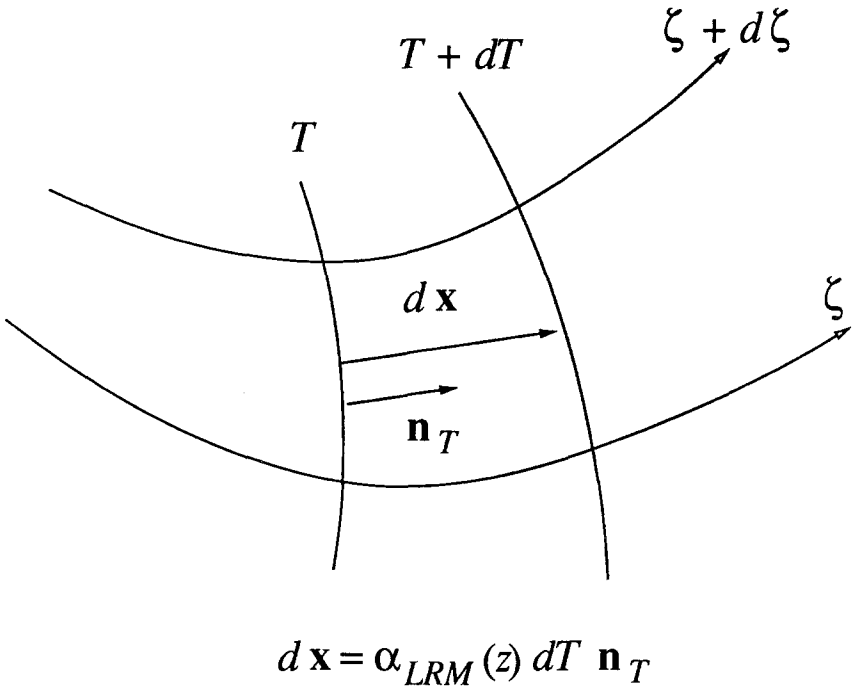

FIG. 3. Schematic diagram defining quantities employed in the derivation of scale factors (a) h_T and (b) h_ζ for a curvilinear ray coordinate system corresponding to a medium with constant velocity gradient.

We can derive analytic expressions for these scale factors by considering the nature of a differential element in (T, ζ) space as shown in Figure 3a. The scale factor h_T can be determined by recognizing that, with the passage of an incremental period of time dT, the wavefront in the LRM moves a distance $d\mathbf{x}$ where

$$d\mathbf{x} = \alpha_{LRM}(z)dT\mathbf{n}_T, \tag{22}$$

and $d\mathbf{x}$ is in the direction of the normal to the wavefront $\mathbf{n}_T$. Hence the scale factor for our curvilinear coordinate T is just the local reference velocity, $\alpha_{LRM}(z) = \alpha_{LRM}(T, \zeta)$,

$$h_T = \alpha_{LRM}(T, \zeta). \tag{23}$$

To determine the scale factor h_ζ corresponding to our transverse coordinate ζ we refer to Figure 3b and note that an incremental change in ζ can be related to a corresponding change in depth dz by the relation

$$h_\zeta = \frac{-1}{\sin(\xi)}\frac{dz}{d\zeta}. \tag{24}$$

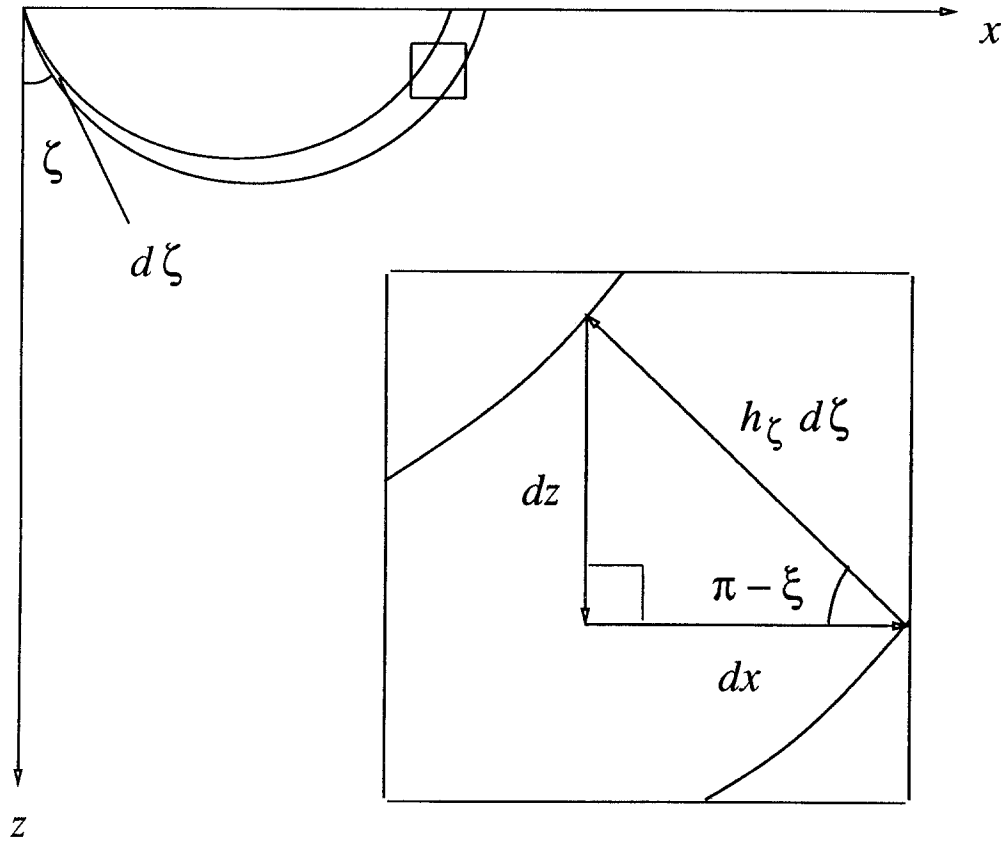

b.

FIG. 3. Continued.

To maintain simplicity we will assume that the origin of our reference frame is located at the origin of a Cartesian coordinate system (i.e., $z = 0$) in which case we can write ξ, the local angle to the vertical of a ray with initial angle ζ at some time T, as

$$\xi = 2\,\mathrm{atan}[\exp(mT)\tan(\zeta/2)]. \tag{25}$$

Likewise the depth z at a given time T in this case is

$$z = \frac{\alpha_{LRM}}{m}\left(\frac{\sin(\xi)}{\sin(\zeta)} - 1\right). \tag{26}$$

With expressions for h_T and h_ζ now in hand, we may look more closely at deriving a parabolic approximation to our original equation (14) which we can rewrite after multiplying by h_T^2 as

$$\left[\frac{\partial^2\theta}{\partial T^2} + \left(h_T f_T - \frac{1}{X}\frac{\partial X}{\partial T}\right)\frac{\partial\theta}{\partial T} + X^2\frac{\partial^2\theta}{\partial\zeta^2} + X\left(h_T f_\zeta - \frac{\partial X}{\partial\zeta}\right)\frac{\partial\theta}{\partial\zeta}\right]$$

$$= [1 + \delta]\frac{\partial^2\theta}{\partial t^2}. \tag{27}$$

For simplicity of the resulting expressions we have chosen to write the velocity $\alpha(x, z)$ in the actual medium in terms of a perturbation parameter $\delta(x, z)$ where $\alpha = h_T/(1 + \delta)^{1/2}$. In addition, we have employed the abbreviated variables

$$f_T = (2\mathbf{g}_\alpha + \mathbf{g}_\rho)\cdot\mathbf{n}_T, \tag{28}$$

$$f_\zeta = (2\mathbf{g}_\alpha + \mathbf{g}_\rho)\cdot\mathbf{n}_\zeta, \tag{29}$$

$$X(T, \zeta) = \frac{h_T}{h_\zeta}. \tag{30}$$

We now follow the same line of argument as that made in the previous section. In particular we assume negligible backscattering ($L \gg \Lambda$) and adopt a retarded time coordinate $\tau = t - T$, which allows us to monitor the slowly varying character of our waveform Θ as it propagates through a heterogeneous region. From the chain rule our differential operators become

$$T \to T', \qquad \frac{\partial}{\partial T} \to \frac{\partial}{\partial T'} - \frac{\partial}{\partial\tau}. \tag{31}$$

and

$$t \to \tau, \qquad \frac{\partial}{\partial t} \to \frac{\partial}{\partial\tau}. \tag{32}$$

Dropping the primes on the variable T' and employing these relations, our wave equation may be written as

$$\left[\frac{\partial^2\Theta}{\partial T^2} - 2\frac{\partial^2\Theta}{\partial\tau\,\partial T} + \left(h_T f_T - \frac{1}{X}\frac{\partial X}{\partial T}\right)\left(\frac{\partial\Theta}{\partial T} - \frac{\partial\Theta}{\partial\tau}\right)\right.$$

$$\left. + X^2\frac{\partial^2\Theta}{\partial\zeta^2} + X\left(h_T f_\zeta + \frac{\partial X}{\partial\zeta}\right)\frac{\partial\Theta}{\partial\zeta}\right] = \delta\frac{\partial^2\Theta}{\partial\tau^2}. \tag{33}$$

Henceforth we follow the same arguments employed in the previous section with respect to scale analysis and discard factors proportional to $1/L^2$. This yields the following parabolic equation

$$\left[2\frac{\partial^2\Theta}{\partial\tau\,\partial T} + \left(h_T f_T - \frac{1}{X}\frac{\partial X}{\partial T}\right)\frac{\partial\Theta}{\partial\tau} - X^2\frac{\partial^2\Theta}{\partial\zeta^2} - Xh_T f_\zeta\frac{\partial\Theta}{\partial\zeta} + \delta\frac{\partial^2\Theta}{\partial\tau^2}\right] = 0. \tag{34}$$

Here we have also dropped a $\partial X/\partial\zeta$ term which in 2D for a constant gradient reference medium is zero.

Numerical Solution

The principal motivation in adopting a parabolic approximation for P-wave propagation is the numerical advantage held over a finite-difference solution of the full hyperbolic wave equation. There are two main reasons for this advantage. First, note that there is only a first derivative dependence in the direction of propagation, hence the solution of equation (34) admits only forward propagating waves and, consequently, we may adopt a relatively coarse grid discretization in this direction. Second, we follow the evolution of the waveform in a reduced time frame τ, and therefore we require a temporal grid which is only as long as the anticipated maximum delay between first- and last-arriving signals that are of interest. Thus the duration of our temporal grid may be only a small fraction of the total time required for the waveform to propagate through a region of heterogeneity.

Similar advantages exist in the frequency domain and considerable effort has been devoted to solving one-way wave equations in exploration seismology where vast quantities of data are frequently involved (see e.g., Claerbout, 1976, 1985). As indicated in previous sections we are interested in a time domain implementation and may choose to solve (34) in one of several ways. One possibility is to employ an efficient and stable algorithm originally proposed by Claerbout and Johnson (1971). In that study, the authors were concerned only with the diffraction of a distorted plane wave propagating in a homogeneous medium. Consequently, they did not need to incorporate terms corresponding to our advective (δ) terms in equations (18) and (34). To apply their algorithm directly would require that we either center the second time difference (corresponding to the $\partial^2\Theta/\partial\tau^2$ term) over a grid point which differs from the center point of the diffraction difference operator, or split the total equation into two separate parts, a diffraction part and a "thin lens" or advective part, and solve these in alternate steps. We have chosen a third approach where all differences are centered over the same point and which avoids splitting. This involves integrating (34) over reduced time τ from negative infinity to our point of interest τ'.

$$\int_{-\infty}^{\tau'} d\tau \left[2\frac{\partial^2\Theta}{\partial\tau\,\partial T} + \left(h_T f_T - \frac{1}{X}\frac{\partial X}{\partial T} \right)\frac{\partial\Theta}{\partial\tau} - X^2\frac{\partial^2\Theta}{\partial\zeta^2} - Xh_T f_\zeta \frac{\partial\Theta}{\partial\zeta} + \delta\frac{\partial^2\Theta}{\partial\tau^2} \right]$$

$$= \left[2\frac{\partial\Theta}{\partial T} + \left(h_T f_T - \frac{1}{X}\frac{\partial X}{\partial T} \right) - X^2\frac{\partial^2}{\partial\zeta^2}\int_{-\infty}^{\tau'} d\tau\Theta \right.$$

$$\left. - Xh_T f_\zeta \frac{\partial}{\partial\zeta}\int_{-\infty}^{\tau'} d\tau\Theta + \delta\frac{\partial\Theta}{\partial\tau} \right]. \tag{35}$$

We note that the $\partial\Theta/\partial\zeta$ and $\partial^2\Theta/\partial\zeta^2$ operators commute with the $\int_{-\infty}^{\tau'} d\tau$ operator and that none of the geometrical factors involving X or the material property gradients depend on τ. Thus we have transformed (34) into a integro-differential equation which may be solved using a combination of finite-differencing and numerical quadrature. To do this we employ a discretized dilatation $\Theta_{j,k}^n$ where $T = n\,\Delta T$, $\tau = j\,\Delta\tau$, and $\zeta = k\,\Delta\zeta$. Our initial condition involves a waveform of finite duration prescribed as a function of reduced time τ and introduced to our upper mantle model at some boundary level in our LRM

coordinate frame, $T = T_0$. Since we have purposely chosen our reference medium LRM to exhibit velocities which are everywhere slightly greater than those in the actual medium of propagation, we know that the value of $\Theta_{j,k}^{n}$ on our temporal grid will always be zero in advance of some prescribed value of τ ($j = 1$ in our finite-difference scheme). This formulation allows us to derive a stable, implicit finite-difference scheme for the unknown $\Theta_{j+1,k}^{n+1}$ in terms of known $\Theta_{j,k}^{n+1}$, $\Theta_{j+1,k}^{n}$, and $\Theta_{j,k}^{n}$ centered over the point $(n + \frac{1}{2}, j + \frac{1}{2})$. The derivatives in T and τ at this point are differenced as

$$\frac{\partial \Theta}{\partial T} \approx \frac{\Theta_{j+1,k}^{n+1} - \Theta_{j,k}^{n+1} + \Theta_{j+1,k}^{n} - \Theta_{j,k}^{n}}{2\Delta T}, \tag{36}$$

$$\frac{\partial \Theta}{\partial \tau} \approx \frac{\Theta_{j+1,k}^{n+1} - \Theta_{j+1,k}^{n} + \Theta_{j,k}^{n+1} - \Theta_{j,k}^{n}}{2\Delta \tau}. \tag{37}$$

We can approximate the integral over reduced time to the point (n, j) using the trapezoidal rule operator S where

$$\int_{-\infty}^{\tau'} d\tau \Theta \approx S(\Theta_{j,k}^{n}) \equiv \Delta\tau \left(\sum_{i=1}^{j-1} \Theta_{i,k}^{n} + \frac{\Theta_{j,k}^{n}}{2} \right), \tag{38}$$

We approximate Θ as

$$\Theta \approx \frac{\Theta_{j+1,k}^{n+1} + \Theta_{j,k}^{n+1} + \Theta_{j+1,k}^{n} + \Theta_{j,k}^{n}}{4}, \tag{39}$$

so that the value of the integral to the point $(n + \frac{1}{2}, j + \frac{1}{2})$ is approximately

$$\begin{aligned} &\frac{S\left(\Theta_{j+1,k}^{n+1}\right) + S\left(\Theta_{j,k}^{n+1}\right) + S(\Theta_{j+1,k}^{n}) + S(\Theta_{j,k}^{n})}{4} \\ &\quad = \frac{S\left(\Theta_{j,k}^{n+1}\right) + S(\Theta_{j,k}^{n})}{2} + \frac{\Theta_{j+1,k}^{n+1} + \Theta_{j,k}^{n+1} + \Theta_{j+1,k}^{n} + \Theta_{j,k}^{n}}{8}. \end{aligned} \tag{40}$$

Finally we represent our derivative operators in the transverse direction ζ through the finite-difference operators Λ_k and Π_k where

$$\Lambda_k(\Theta_{j,k}^{n}) = \frac{\Theta_{j,k+1}^{n} - 2\Theta_{j,k}^{n} + \Theta_{j,k-1}^{n}}{(\Delta\zeta)^2}, \tag{41}$$

$$\Pi_k(\Theta_{j,k}^{n}) = \frac{\Theta_{j,k+1}^{n} - \Theta_{j,k-1}^{n}}{2\Delta\zeta}. \tag{42}$$

The complete finite-difference representation of (35) is then written as

$$\begin{aligned} &\left[1 + A_k^{\,n+1/2} + B_k^{\,n+1/2} - C_k^{\,n+1/2} - D_k^{\,n+1/2}\right]\Theta_{j+1,k}^{n+1} \\ &\quad = \left[-1 - A_k^{\,n+1/2} + B_k^{\,n+1/2} + C_k^{\,n+1/2} + D_k^{\,n+1/2}\right]\Theta_{j,k}^{n+1} \\ &\qquad + \left[1 - A_k^{\,n+1/2} - B_k^{\,n+1/2} + C_k^{\,n+1/2} + D_k^{\,n+1/2}\right]\Theta_{j+1,k}^{n} \\ &\qquad + \left[1 - A_k^{\,n+1/2} + B_k^{\,n+1/2} + C_k^{\,n+1/2} + D_k^{\,n+1/2}\right]\Theta_{j,k}^{n} \\ &\qquad + 4\left[C_k^{\,n+1/2} + D_k^{\,n+1/2}\right]\left[S(\Theta_{j,k}^{n}) + S\left(\Theta_{j,k}^{n+1}\right)\right], \end{aligned} \tag{43}$$

where we have employed the discretized quantities

$$A_k^{n+1/2} = \frac{\Delta T}{4}\left(f_T - \frac{1}{X}\frac{\partial X}{\partial T}\right)_k^{n+1/2}, \tag{44}$$

$$B_k^{n+1/2} = \frac{\Delta T}{2\Delta\tau}(\delta)_k^{n+1/2}, \tag{45}$$

$$C_k^{n+1/2} = \frac{\Delta T\,\Delta\tau}{8}(X^2)_k^{n+1/2}\Lambda_k, \tag{46}$$

$$D_k^{n+1/2} = \frac{\Delta T\,\Delta\tau}{16}(Xf_\zeta)_k^{n+1/2}\Pi_k. \tag{47}$$

The issue of boundary conditions must also be considered. We might choose to implement some form of absorbing boundary condition (see Clayton and Engquist, 1980) expressed in curvilinear coordinates. However it is simpler to recognize that, in our application, artificial reflections from grid boundaries will arrive at times which are significantly later than the portion of the seismogram we are interested in. Hence it is most economical to employ simple two-point Dirichlet or Neumann boundary conditions.

Thus if we consider $\Theta_{j,k}^n$ as a vector in k, then we can view equation (43) as a matrix equation where $\Theta_{j+1,k}^{n+1}$ represent our unknowns, with all remaining quantities on the right hand side known and calculable. Further note that the matrix system on the left hand side of (43) is tridiagonal and so we can exploit the Crank-Nicholson scheme for its solution. The solution proceeds by solving (43) first for all $j = 0, J$ on our temporal grid at a given value of n, and then repeating this process for all further values of n.

To summarize, our strategy will be to consider a given incident waveform at some initial boundary T_0 on our LRM grid. We then forward propagate this waveform using (43) to some desired level in our upper mantle model, generally the Earth's surface. Although our method requires that the magnitude and wavelength of the heterogeneity is such that backward scattering is small, we have incorporated terms which describe diffraction effects such as wavefront healing. For this reason we expect to gain a better understanding of frequency-dependent effects on teleseismic P waves propagating through a subduction zone than is possible, for example, by using high-frequency asymptotic methods. In the following section we examine the effect of a model slab on synthetic long- and short-period P waveforms.

Numerical Examples

In this section we examine P-wave propagation in an upper mantle model of a subduction zone using the parabolic approximation developed in earlier sections. Our interest is motivated, in part, by work currently in progress to monitor teleseismic P-wave distortion caused by the Cascadia slab as recorded on the Washington regional seismograph network. In a companion paper we compare observations with synthetic seismograms for models of Cascadia derived from travel time inversion studies and which serve as realistic representations of the expected structure in this complicated region. For the present study, however, our main concern will be to demonstrate the application of the method, and identify some of the important physical interactions that take place be-

tween the wave field and the subducted slab at high and low frequencies. To this end, we will confine our attention to a simple 2D slab model where the heterogeneity exists as a perturbation on a reference medium with velocity profile which is linearly dependent on depth.

To model this situation we will consider an incoming teleseismic wave introduced at some initial level in our mantle model and examine its expression at the surface after propagation through the slab structure. The reference medium is characterized by the velocity profile

$$\alpha(x, z) = 0.00412z + 7.9 \tag{48}$$

which provides a reasonable representation of an average velocity profile in many upper mantle models (see Figure 2). Note here that units of distance and velocity are *km* and *km/sec*, respectively. For our initial wave field we select the ray theoretical solution for a surface point source and a medium with velocity profile as in (48). This is readily calculated analytically by solving the transport equation associated with the scalar wave equation in (14). The slab is modeled as a 2D tabular body comprising a +5% Gaussian perturbation on top of the reference medium with a width at 1/e of maximum value of 70 km and extending to 400 km depth as shown in Figure 4. The axial plane of the slab is oriented at a dip of 55° and intersects the surface at a distance of approximately 6400 km from the source. The finite difference grid on which we solve (34) is defined by boundary rays in the reference medium which leave the source at angles, ζ, of approximately 29.5 and 32.5° and which reach the surface at distances between 6000 and 7000 km. A portion of the grid is shown schematically in Figure 5 and illustrates the class of wave field-slab configuration which

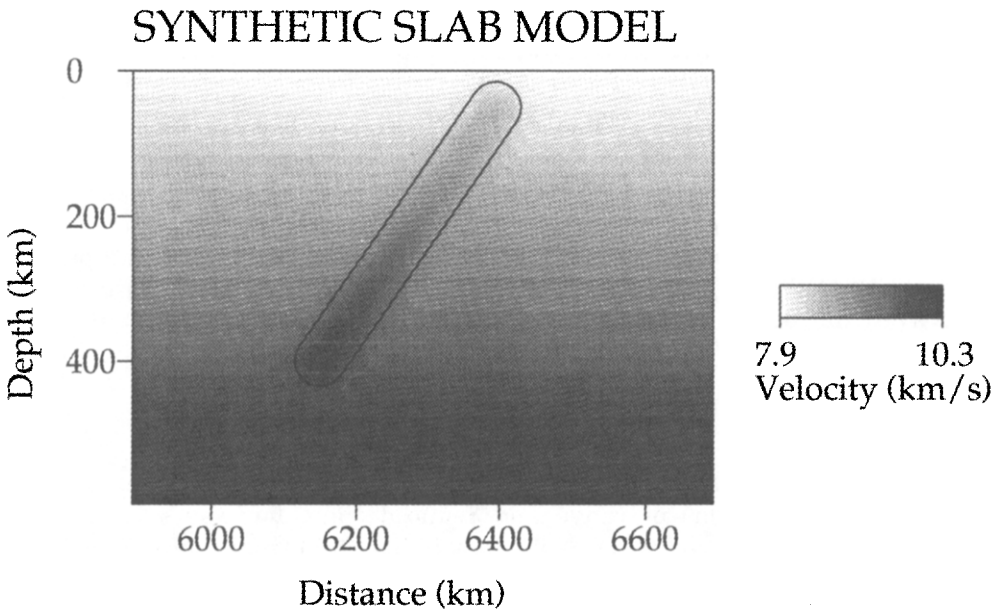

FIG. 4. Synthetic slab model for the numerical examples described in Sections 7 and 8. The slab is represented by a 2D tabular body extending between 50 and 400 km depth. The velocity profile across the axial plane of the slab is a 5% Gaussian positive velocity perturbation with a half width of 40 km.

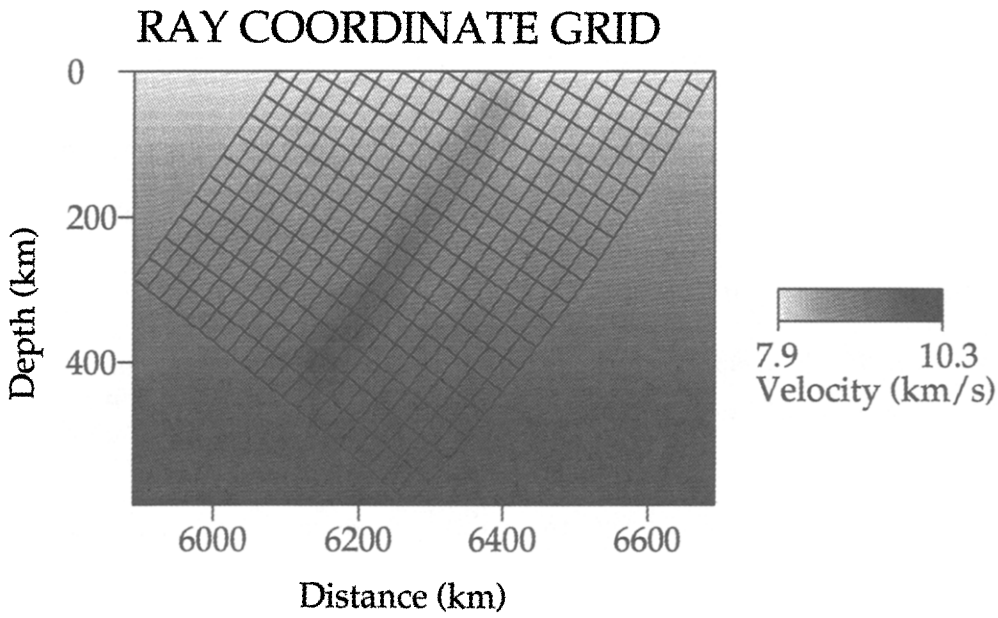

FIG. 5. Schematic representation of the finite-difference grid employed to solve the parabolic equation (35) for the slab model described in Section 7. The grid is superimposed on a grayscale map of the velocity field.

we wish to investigate. In particular, we examine the case where the wave field propagates roughly parallel to the axial plane of the slab. For strictly 2D geometries we expect the most severe waveform distortions to result from this configuration.

The incident waveform employed in the next section for high-frequency study is a simple Gaussian pulse defined by

$$w(\tau, \zeta) = A(\zeta)\exp\left[-12(\tau - 0.625)^2\right] \tag{49}$$

where $A(\zeta)$ is the geometric amplitude along the wavefront, τ is measured in seconds. Although not particularly realistic, Gaussian waveforms are attractive (see Vidale, 1987; Cormier, 1989) in their simplicity and symmetry, and permit a straightforward analysis of pulse distortion. The spectrum of the pulse in (49) is relatively flat between 0 and 1.0 Hz and has dropped well below 20 dB after 2.0 Hz. We use a similar pulse scaled in time to describe lower frequency propagation.

HIGH FREQUENCY PROPAGATION

Figure 6 shows a series of synthetic seismograms as recorded at the surface and plotted as functions of range and reduced time, for waves containing significant energy out to 1.0 Hz. Note that higher frequencies here will have propagated distances through the anomalous region to the surface in excess of 60 wavelengths. Several features are immediately apparent, in particular the negative travel time anomaly associated with that portion of the wave field that has propagated up the high-velocity slab. For the model parameters we have chosen to adopt this anomaly ranges up to approximately 3 sec and is most

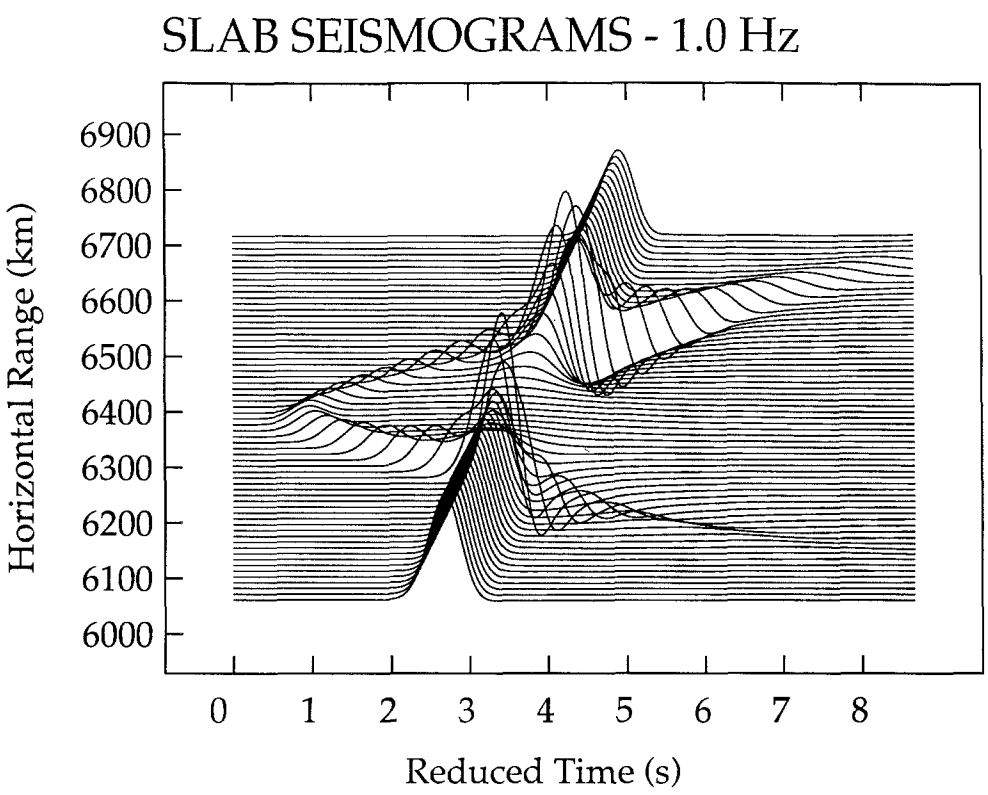

FIG. 6. Short-period synthetic seismograms recorded at the surface over the slab model (see Figure 4). At higher frequencies multipathing of ray geometric arrivals is the principal factor affecting waveform distortion.

pronounced at 6400 km where the axial plane of the slab intersects the surface. The effect of the slab is also witnessed in the amplitudes of the waveforms: since the slab represents a region of increased velocity it behaves as an anti-wave guide (see Gubbins and Snieder, 1991) which continuously refracts energy out of its borders. Thus there is a systematic loss of energy from that portion of the wave field which propagates up the core of the slab as illustrated in Figure 6. The most severely affected waves exhibit amplitudes which are approximately one sixth those in the undistorted wave field recorded at the surface.

Perhaps the most interesting effect is observed on seismograms which record waves that have traveled to either side of the slab axis and interacted with the more pronounced transverse velocity gradients. In these regions we note a complicated distortion in the waveform which results, in geometrical optics terms, from a triplication and the consequent interference of three separate phases. A smaller selection of traces is shown in Figure 7 to indicate more clearly the nature of these phases. Above the slab in the range 6240 to 6310 km and below the slab between 6471 to 6566 km we can identify the interference of the direct wave and a second Hilbert transformed phase which has touched the caustic surface. The expression of this interference is sensitive to position and varies rapidly over relatively short distances. At certain positions the interference results in amplitudes that are approximately twice those in the undisturbed wave field. The observation and interpretation of this phenomenon in

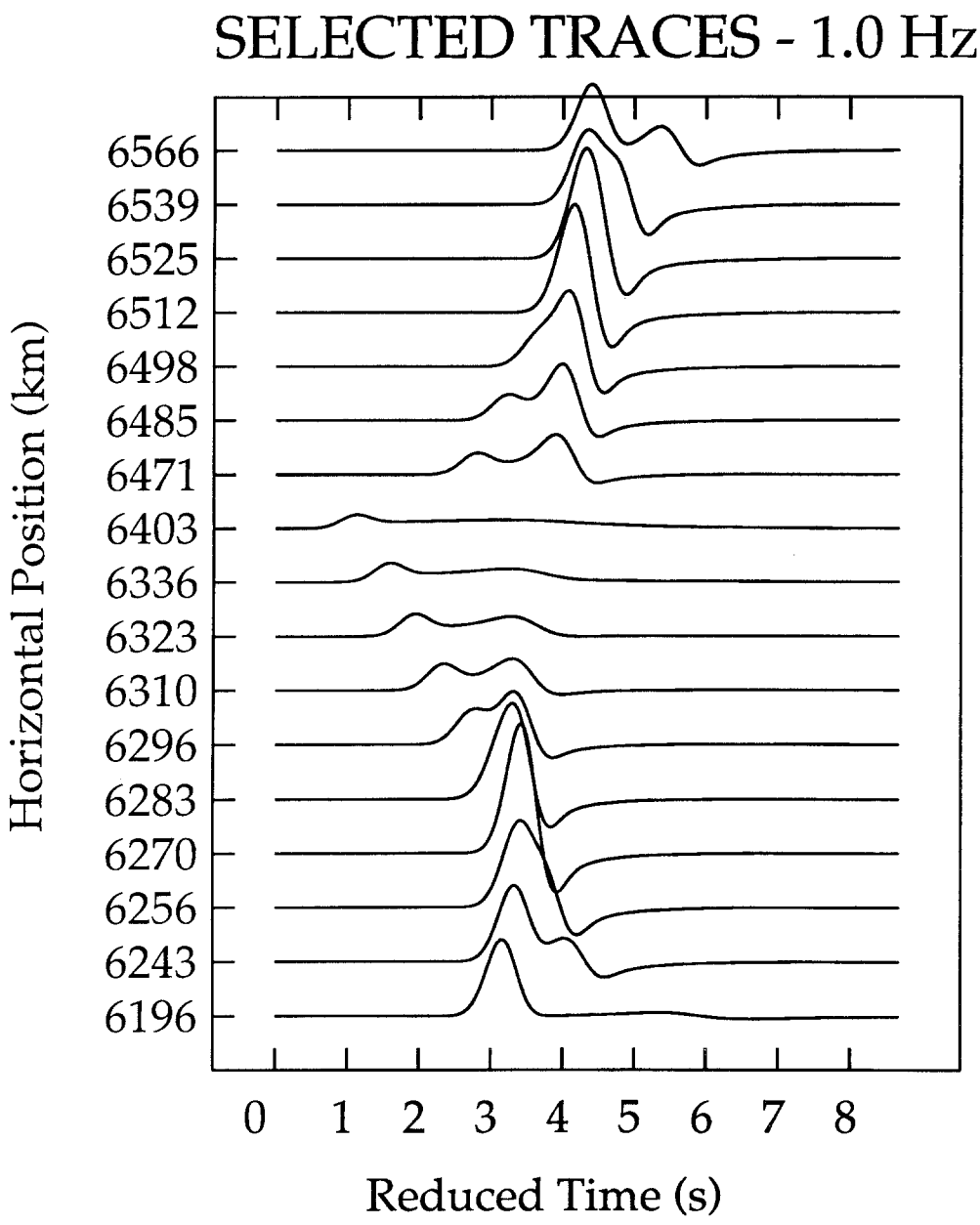

FIG. 7. Selected short-period synthetics at various locations across the slab. Note the interference between the direct arrival and the Hilbert transformed pulse which has touched the caustic surface.

actual data would require a high density of recording stations. The pattern of waveform distortion about the axial plane of the slab is, of course, asymmetric owing to the geometry of the problem. In particular this asymmetry can be seen to arise from several different and competing factors: i) the velocity gradient above the slab is greater than that below; ii) the wave field below the slab propagates a greater distance through the anomalous region before reaching the surface than that above; and iii) the initial conditions require that our starting

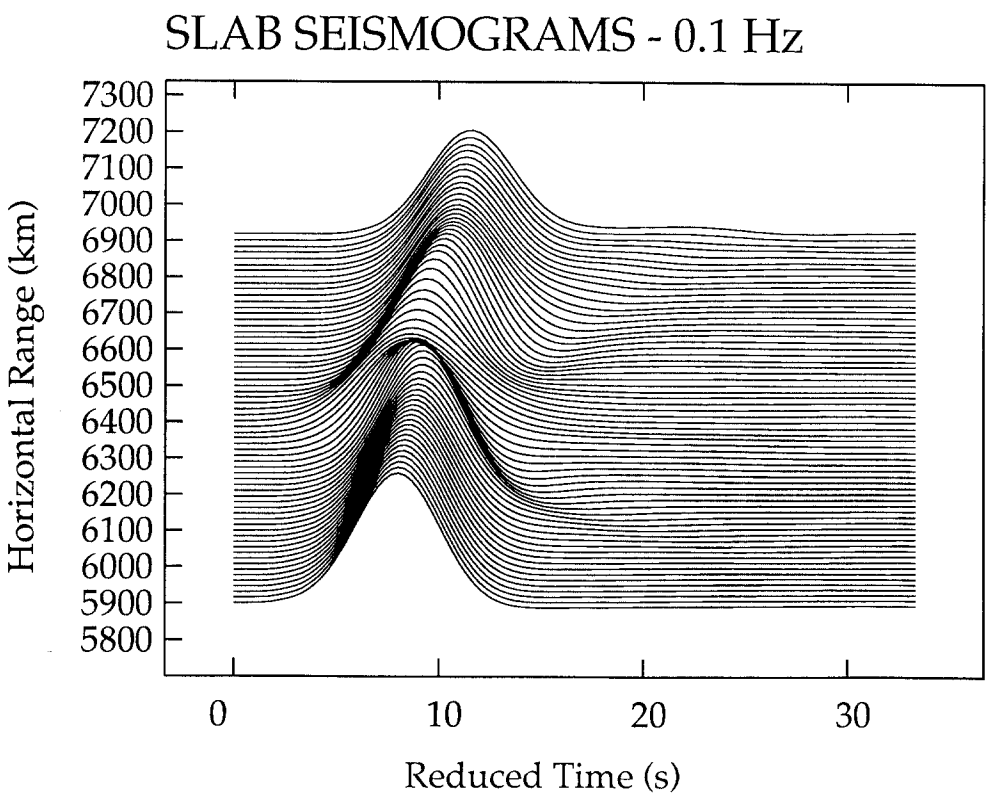

FIG. 8. Long-period synthetic seismograms recorded at the surface over the slab model. At lower frequencies diffraction of the waveform becomes an important factor in determining the character of waveform distortion.

wave field vary slightly in amplitude along the wavefront as indicated in (49). These factors result in slightly greater peak amplitudes above the slab than below and a difference in the moveout of the secondary phases on either side of the slab.

Finally, we note that the lower frequencies in the waveform experience noticeable diffraction. This is apparent in Figure 7 for seismograms at 6323, 6336, and 6403 km wherein it is apparent that a very low-amplitude, low-frequency component of energy follows the first arrival. This results from a "leakage" of energy into the slab from the external medium. The nature of the distortion in the lower frequencies is examined in the following section.

LOW-FREQUENCY PROPAGATION

We now investigate the effect of the same model slab on a wave field which contains significant energy over a narrower frequency band. The shape of the incident pulse is the same as that in the previous example, however it has been stretched in time by a factor of 10 so that most of its energy is confined to the band 0 to 0.1 Hz. Although the appearance of the section in Figure 6 differs quite markedly from that in Figure 8, there are several broad similarities (note that the time axis has changed). First, the same general negative travel time anomaly exists over that portion of the wave field which has propagated up the high-velocity slab. Second, the amplitudes of corresponding waveforms are

reduced relative to those in the unaffected portion of the wave field. Here the similarities end; the wave field at longer periods is far more severely affected by the frequency-dependent effect of the diffraction operator in equation (34). Since it is expressed through the second derivative transverse to the general direction of propagation, this operator has a smearing or averaging effect and tends to heal the sharper, more pronounced features in the wave field. Thus we find that severe waveform distortion observed in the previous example via multipathing is no longer present. For example the variation in amplitude is more subdued, ranging between 75 to 110% of the value expected for the unperturbed, laterally homogeneous reference medium. In addition, rather than observing the evolution of distinct phases, we find that the waveforms see the effect of the slab in terms of a broadening, or an increase in low-frequency content (see Figure 9). This is most pronounced for waveforms traveling up the axial plane of the slab since the early component of the waveform has propagated through the high-velocity slab material and later energy arrives via leakage of the energy into the slab from the slower, external wave.

Discussion and Conclusions

We have presented a method for computing time domain synthetic seismograms for P waves propagating in a laterally heterogeneous upper mantle. The method describes distortion over the initial few cycles of the P waveform and requires that material contrasts be smooth on the scale of a wavelength such that backscattered energy is negligible. In this case we can derive a parabolic approximation to the wave equation in which the principal processes affecting the pulse during propagation are explicitly identified. These include advection (i.e., time delay or advance of the pulse), growth or decay of the waveform amplitude, and diffraction which smoothes the wave field and is strongly dependent on frequency.

In order to implement the parabolic approximation we must identify *a priori* a coordinate system which mimics the general flow of energy. A reasonably accurate representation of a reference velocity structure in the upper mantle is afforded by a profile which is linear in depth. This motivates our solution of the parabolic equation on a curvilinear coordinate grid where the orthogonal coordinates are simply the rays and wavefronts for a point source in a reference medium with constant velocity gradient. The result is an efficient forward propagator scheme which involves integrating the parabolic equation using finite differences forward in space from some initial level, through a region of heterogeneity, to the Earth's surface.

Application of the method to a simple 2D slab model demonstrates the contrasting effects of the slab anomaly on high- and low-frequency waves. At short periods we observe the effects predicted from ray theory, notably advanced travel times and reduced amplitudes for waves traveling up the axial plane of the slab, and the complex interference of multipathed arrivals away from the axial plane. Long-period waves exhibit the same qualitative travel time and amplitude characteristics; however, the character of waveform distortion differs quite markedly. Wave diffraction plays an important role in this case and results in a wave field which exhibits more gradual variations. In particular we find that waveforms which have propagated through the slab anomaly are characterized primarily by broadening, or equivalently an increase in low-frequency content.

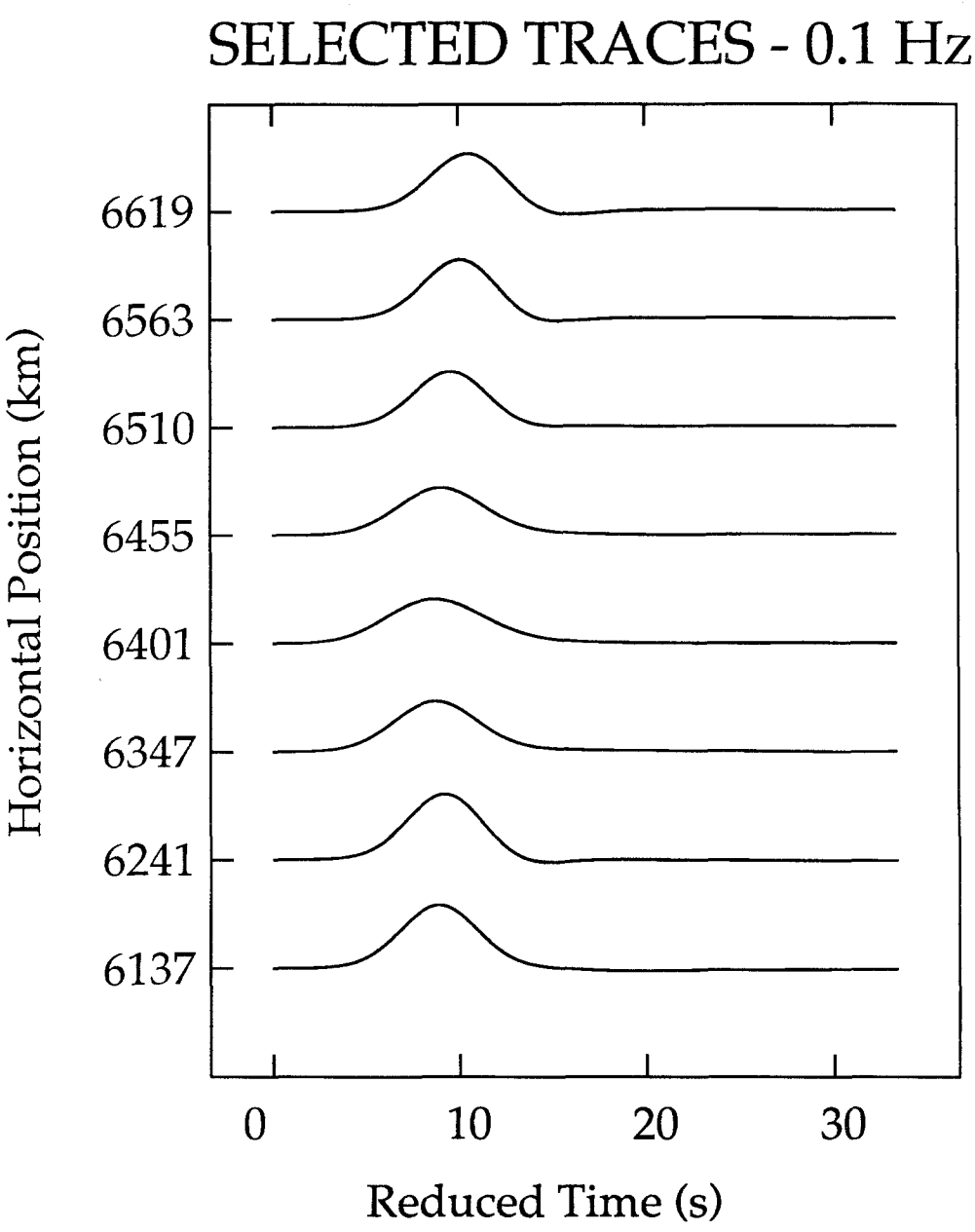

FIG. 9. Selected long-period synthetics at various locations across the model slab. Wave diffraction causes a "leakage" of energy into the high velocity slab corridor and results in a broadening of the waveform.

Research is currently under way into applying the parabolic approximation in the form derived here to more accurate realizations of *P*-wave propagation in a laterally heterogeneous upper mantle. This includes the incorporation of more realistic velocity models, notably the Cascadia slab model of VanDecar (1991) constructed through the inversion of teleseismic travel time data. This will in turn allow for a comparison of synthetic waveforms with actual field data. The inclusion of velocity discontinuities is also contemplated and requires that these

be identified explicitly in the finite difference scheme. In addition we are investigating the extension of the method to 3D heterogeneity. The theory for 3D follows trivially from the derivation presented here for 2D situations; the complication arises in the development of a numerical implementation which is both accurate and computationally efficient. As in related applications (Claerbout, 1973, 1985), it is no longer practical to difference the parabolic equation in an implicit manner and therefore explicit treatments must be adopted which do not suffer too severely from the effects of numerical dispersion.

ACKNOWLEDGMENTS

This research was supported by the Netherlands Organization for Scientific Research (NWO) through the Pionier project PGS 76–144. J. C. V. was funded through National Science Foundation Grant INT–9102113.

REFERENCES

Aki, K. and P. G. Richards (1980). *Quantitative Seismology: Theory and Methods*, W. H. Freeman, New York.

Ben-Menahem, A. and W. B. Beydoun (1985). Range of validity of seismic ray and beam methods in general inhomogeneous media—I. General theory, *Geophys. J. R. Astr. Soc.* **82,** 207–234.

Cerveny, V. and K. Psencik (1983). Gaussian beams and paraxial ray approximation in three-dimensional elastic inhomogeneous media, *J. Geophys.* **53,** 1–15.

Claerbout, J. F. (1970). Coarse grid calculations of waves in inhomogeneous media with application to delineation of complicated seismic structure, *Geophysics* **35,** 407–418.

Claerbout, J. F. (1976). *Fundamentals of Geophysical Data Processing*, McGraw-Hill, New York.

Claerbout, J. F. (1985). *Imaging the Earth's Interior*, Blackwell Scientific Publications, Oxford.

Claerbout, J. F. and A. G. Johnson (1971). Extrapolation of time-dependent waveforms along their path of propagation, *Geophys. J. R. Astr. Soc.* **26,** 285–293.

Clayton, R. W. and B. Enquist (1980). Absorbing side boundary conditions for wave-equation migration, *Geophysics* **45,** 895–904.

Cormier, V. F. (1989). Slab diffraction of *S* waves, *J. Geophys. Res.* **96,** 6321–6333.

Davies, D. and B. R. Julian (1972). A study of short period *P*-wave signals from Longshot, *Geophys. J. R. Astr. Soc.* **29,** 185–202.

Gubbins, D. and R. Snieder (1991). Dispersion of *P*-waves in subducted lithosphere: Evidence for an eclogite layer, *J. Geophys. Res.* **96,** 6321–6333.

Haines, A. J. (1983). A phase-front method—I. Narrow frequency band *SH*-waves, *Geophys. J. R. Astr. Soc.* **72,** 783–808.

Haines, A. J. (1984a). A phase-front method—II. Broad frequency band *SH*-waves, *Geophys. J. R. Astr. Soc.* **77,** 43–64.

Haines, A. J. (1985b). A phase-front method—III. Acoustic waves, *P*- and *S*-waves, *Geophys. J. R. Astr. Soc.* **77,** 65–103.

Landers, T. and J. F. Claerbout (1972). Numerical calculations of elastic waves in laterally inhomogeneous media, *J. Geophys. Res.*, **77,** 1476–1482.

Lay, T. (1991). Mantle structure: A matter for resolution, *Nature*, **352,** 105.

Silver, P. G., R. W. Carlson, and P. Olson (1988). Deep slabs, geochemical heterogeneity, and the large scale structure of mantle convection: Investigation of an enduring paradox, *Annu. Rev. Earth Planet. Sci.* **16,** 477–541.

Silver, P. G. and W. W. Chan (1986). Observations of body-wave multipathing from broad-band seismograms: Evidence for lower mantle slab penetration beneath the Sea of Okhotsk, *J. Geophys. Res.* **91,** 13787–13802.

Sleep, N. H. (1973). Teleseismic *P*-wave transmission through slabs, *Bull. Seism. Soc. Am.* **63,** 1349–1373.

Spakman, W. (1991). Delay-time tomography of the upper mantle below Europe, the Mediterranean and Asia Minor, *Geophys. J. Int.* **107,** 309–332.

Thomson, C. J. and D. Gubbins (1982). Three-dimensional lithospheric modelling at NORSAR: linearity of the method and amplitude variations from the anomalies, *Geophys. J. R. Astr. Soc.* **71,** 1–36.

VanDecar, J. C. (1991). Upper-mantle structure of the Cascadia subduction zone from non-linear teleseismic travel-time inversion. *Ph.D. Thesis*, University of Washington, Seattle.

VanDecar, J. C. and R. S. Crosson (1990). Determination of teleseismic relative phase arrival times using multi-channel cross correlation and least squares, *Bull. Seism. Soc. Am.* **80,** 150–169.

VanDecar, J. C., R. S. Crosson, and K. C. Creager (1990). Teleseismic arrivals recorded over the Cascadia Subduction Zone: Amplitude variation and calibration of the Washington Regional Seismic Network (abstract), *Seism. Res. Lett.* **61,** 32.

Vidale, J. E. (1987). Waveform effects of a high-velocity, subducted slab, *Geophys. Res. Lett.* **14,** 542–545.

Vidale, J. E. and D. Garcia-Gonzalez (1988). Seismic observation of a high-velocity slab 1200–1600 km in depth, *Geophys. Res. Lett.* **15,** 369–372.

DEPARTMENT OF THEORETICAL GEOPHYSICS
UTRECHT UNIVERSITY
P.O. BOX 80.021
3508 TA UTRECHT
THE NETHERLANDS

GEOPHYSICS PROGRAM
UNIVERSITY OF WASHINGTON
SEATTLE, WASHINGTON
(J.C.V.)

Manuscript received June 22, 1992